

On the performance limits of coatings for gravitational wave detectors made of alternating layers of two materials

V. Pierro^{a,g}, V. Fiumara^{b,g}, F. Chiadini^{c,g}, F. Bobba^{d,g}, G. Carapella^{d,g}, C. Di Giorgio^{d,g}, O. Durante^{d,g}, R. Fittipaldi^{e,g}, E. Mejuto Villa^{a,g}, J. Neilson^{a,g}, M. Principe^{d,f,g}, I. M. Pinto^{a,f,g}

^a*Dipartimento di Ingegneria, Università del Sannio, I-82100 Benevento, Italy.*

^b*Scuola di Ingegneria, Università della Basilicata, I-85100 Potenza, Italy.*

^c*Dipartimento di Ingegneria Industriale DIIN, Università di Salerno, I-84084 Fisciano, Salerno, Italy.*

^d*Dipartimento di Fisica "E.R. Caianiello", Università di Salerno, I-84084 Fisciano, Salerno, Italy.*

^e*CNR-SPIN, c/o Università di Salerno, I-84084 Fisciano, Salerno, Italy.*

^f*Museo Storico della Fisica e Centro Studi e Ricerche "Enrico Fermi", I-00184 Roma, Italy.*

^g*INFN, Sezione di Napoli Gruppo Collegato di Salerno, Complesso Universitario di Monte S. Angelo, I-80126 Napoli, Italy.*

Abstract

The coating design for mirrors used in interferometric detectors of gravitational waves currently consists of stacks of two alternating dielectric materials with different refractive indexes. In order to explore the performance limits of such coatings, we have formulated and solved the design problem as a multiobjective optimization problem consisting in the minimization of both coating transmittance and thermal noise. An algorithm of global optimization (Borg MOEA) has been used without any *a priori* assumption on the number and thicknesses of the layers in the coating. The algorithm yields to a Pareto tradeoff boundary exhibiting a continuous, decreasing and non convex (bump-like) profile, bounded from below by an exponential curve which can be written in explicit closed form in the transmittance-noise plane. The lower bound curve has the same expression of the relation between transmittance and noise for the quarter wavelength design where the noise coefficient of the high refractive index material assumes a smaller equivalent value. An application of this result allowing to reduce the computational burden of the search procedure is reported and discussed.

Keywords: Dielectric multilayers, Gravitational Wave Interferometric Detectors, Multiobjective optimization

DOI: 10.1016/j.optmat.2019.109269

1. Introduction

The first direct detection of gravitational waves (henceforth GW) by the LIGO [1] and Virgo [2] detectors, and the recent Multi Messenger observation of GW170817 - GRB 170817A - SSS17a/AT 2017gfo marked the birth of Multi Messenger Astronomy (MMA) [3, 4]. Increasing the visibility distance of the operating GW detectors is a needed step to deploy the full potential of MMA. Thermal (Brownian) fluctuations in the high-reflectance (HR) coatings of the test-masses is presently the dominant noise source in interferometric GW detectors [5] setting their

ultimate visibility distance in the (40-300) Hz band, where all recent detections have been made. Notably, efforts to reach and beat the quantum noise limit will be meaningful only after a significant reduction of coating thermal noise is achieved.

Reducing coating thermal noise is thus the top current priority in GW detectors R&D [6]. The current research direction in coating technology explore two promising options for reducing coating thermal noise as needed by new generation detectors, namely the search of new material (e.g. crystalline materials [7] nm-layered composite materials [8], Silicon Nitrides [9, 10] etc.), and the opti-

mization of coating design, and deposition parameters to achieve the best relevant figures of merit (low optical and mechanical losses, high optical contrast).

In this paper we focus on optimization of the coating structure adopted in advanced LIGO and advanced Virgo. High reflectance test-mass coatings consist of multilayers of alternating low and high refractive index materials (silica and 14.5% titania-doped tantala in the advanced LIGO and Virgo [11, 12]), which must provide the required reflectance with minimal thermal noise [13].

High reflectance optical coatings typically consist of a stack of identical high/low index layer pairs or *doublets*, where each layer is quarter wave thick at the operating frequency [11]. This design features the minimum number of layers to achieve some specified reflectance, but does not yield the minimum noise among all possible iso-reflective designs (see [13] chapter 12).

An alternative design consisting of a stack of identical doublets (with the exception of the terminal top/bottom doublets) with non-quarter wave layers was proposed in [14, 15] and further explored in [16], and shown to outperform the classical quarter wavelength design.

In this paper, we formulate for the first time to the best of our knowledge a multiobjective coating optimization problem consisting in the minimization of both coating transmittance and thermal noise. We use a global optimization method (Borg MOEA [17]), making no *a priori* assumptions about layer thicknesses, and we find a simple closed form lower bound of the general coating performance in the transmittance-noise plane. Also, the end-tweaked stacked-doublet coating structure of the *optimized* coatings assumed in [13, 14, 15] on the basis of partial evidences, is obtained in a rigorous way.

In the following an $\exp(i\omega t)$ dependence on time t is implicit, where ω is the angular frequency and i is the imaginary unit.

The paper is organized as follows: in Sect. 2 and 3 we introduce the optical and thermal-noise model. Constrained optimization and the multiobjective formulation are discussed in Sect. 4. The results are collected in Sect. 5, conclusions and recommendations for future research follow in Sect. 6.

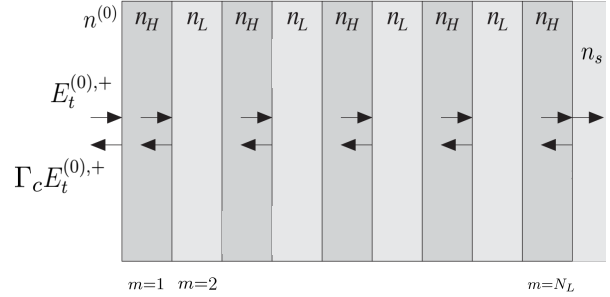


Figure 1: Multilayer structure made of N_L alternating high and low refractive indexes denoted as n_H and n_L respectively, deposited on a substrate of refractive index n_s . The layer index m increases from left to right, the leftmost vacuum half-space corresponds to $m = 0$. The field $E_t^{(0),+}$ is the complex amplitude of the incident electric field (in the frequency domain).

2. Coating optical modeling

Let us consider a coating consisting of a multilayer placed between two homogeneous dielectric half-spaces with refractive indexes $n^{(0)}$ and n_s , respectively (see Fig. 1). The rightmost half-space (with refractive index n_s) is the substrate, while the leftmost one is the vacuum. Let a monochromatic plane wave impinge normally on the coating from the vacuum. The optical reflections and transmission properties of a multilayer structure can be computed in a closed form using the characteristic matrix method [18, 19].

The characteristic matrix of the m -th layer can be written [20]:

$$\mathbf{T}_m = \begin{bmatrix} \cos(\psi_m) & i(n^{(m)})^{-1} \sin(\psi_m) \\ in^{(m)} \sin(\psi_m) & \cos(\psi_m) \end{bmatrix}, \quad (1)$$

where

$$\psi_m = \frac{2\pi}{\lambda_0} n^{(m)} d_m, \quad (2)$$

λ_0 and d_m are the free space wavelength and the layer thickness, respectively, and $n^{(m)}$ is the complex refractive index

$$n^{(m)} = n_r^{(m)} - i\kappa^{(m)} \quad (3)$$

where $\kappa^{(m)}$ is the extinction coefficient¹.

The optical response of the whole coating can be computed from the multilayer characteristic matrix,

$$\mathbf{T} = \mathbf{T}_1 \cdot \mathbf{T}_2 \cdot \dots \cdot \mathbf{T}_{N_L} \quad (4)$$

where N_L is the total number of layers numbered from the vacuum to the substrate as illustrated in Fig. 1.

The complex reflection coefficient Γ_c at the vacuum/coating interface is given by:

$$\Gamma_c = \frac{n^{(0)} - n_c}{n^{(0)} + n_c} \quad (5)$$

where n_c is the effective refractive index of the whole multilayer structure,

$$n_c = \frac{T_{21} + n_s T_{22}}{T_{11} + n_s T_{12}}. \quad (6)$$

The power transmittance at the vacuum/coating interface is $\tau_c = 1 - |\Gamma_c|^2$.

The average power density dissipated within the coating can be computed as the difference between the average power density flowing into the coating at the first interface (vacuum/coating) \mathcal{P}_{in} and the power density flowing into the substrate (last interface) \mathcal{P}_{out} . The input power is

$$\mathcal{P}_{in} = n^{(0)} \frac{1}{2Z_0} |E_t^{(0),+}|^2 \tau_c \quad (7)$$

where $E_t^{(0),+}$ is the incident transverse electrical field at the vacuum/coating interface and $Z_0 = \sqrt{\mu_0/\epsilon_0}$ is the characteristic impedance of the vacuum. The power density flowing into the substrate is given by using the definition of Poynting vector as follow

$$\mathcal{P}_{out} = \frac{1}{2} \Re(E_t^{(N_L)} H_t^{(N_L)*}) \quad (8)$$

where $E_t^{(N_L)}$ and $H_t^{(N_L)}$ are total transverse electric and magnetic fields at the last interface. The complex amplitude $E_t^{(N_L)}$ and $Z_0 H_t^{(N_L)}$ are obtained from $E_t^{(0)} = E_t^{(0),+}(1 + \Gamma_c)$ and $Z_0 H_t^{(0)} = n_T^{(0)} E_t^{(0),+}(1 - \Gamma_c)$ using the formula

$$\begin{bmatrix} E_t^{(N_L)} \\ Z_0 H_t^{(N_L)} \end{bmatrix} = \mathbf{T}^{-1} \begin{bmatrix} E_t^{(0)} \\ Z_0 H_t^{(0)} \end{bmatrix}. \quad (9)$$

¹ In view of the assumed $\exp(i\omega t)$ dependence on the time t , absorbing media have $\kappa^{(m)} > 0$.

3. The thermal noise model

The power spectral density of coating thermal noise is given, under suitable simplifying assumptions, by [13]

$$S_{coat}^B = \frac{2k_B T}{f\pi^{3/2}} \frac{1 - \sigma_s^2}{wY_s} \phi_c \quad (10)$$

where f is the frequency, T is the (absolute) temperature, w is the (assumed Gaussian) laser-beam waist, and σ_s and Y_s are the Poisson and Young modulus of the substrate, and the coating loss angle ϕ_c is

$$\phi_c = \sum_{m=1}^{N_L} \eta_m d_m \quad (11)$$

where

$$\eta_m = \frac{1}{\sqrt{\pi}w} \phi_m \left(\frac{Y_m}{Y_s} + \frac{Y_s}{Y_m} \right) \quad (12)$$

ϕ_m and Y_m being the mechanical loss angle and the Young's modulus of the m -th layer, respectively.

According to eq (10), increasing the beam-width w and lowering the temperature T result in a reduction of coating noise [13]. Using wider (e.g., higher order Gauss-Laguerre) beams is another option, also being currently investigated [21]. Decreasing T works for coating materials that does not exhibit mechanical loss peaks at the (cryo) temperatures of interest [22]. Current research is accordingly focused on finding (synthetizing and optimizing) *better* materials featuring low optical absorption and scattering losses, low mechanical losses down to cryo temperatures, and high optical contrast (allowing fewer layers to achieve a prescribed transmittance, resulting into thinner coatings and lower noise). In this paper we focus on reducing the coating loss angle ϕ_c by optimizing the layer thicknesses.

4. Coating optimization

In this section we focus on the optimization of the coating structure sketched in Fig. 1. Let us use the suffixes S,L,H to identify substrate (S), low (L) and high (H) index material, respectively. In the following we consider a coating consisting of N_L layers beginning with the high refractive index materials² at the vacuum/coating inter-

²This is not restrictive, since the used optimization algorithm is allowed to set the thickness of each and any layer to zero.

face .

As a consequence of the above assumptions

$$\begin{cases} n^{(m)} = n_H - \kappa_H, m \text{ odd}, & n^{(m)} = n_L - \kappa_L, m \text{ even}; \\ \phi_m = \phi_H, m \text{ odd}, & \phi_m = \phi_L, m \text{ even}; \\ Y_m = Y_H, m \text{ odd}, & Y_m = Y_L, m \text{ even}. \end{cases} \quad (13)$$

With this assumptions the coating noise angle becomes:

$$\phi_c = \eta_H \sum_{m \in J_o} d_m + \eta_L \sum_{m \in J_e} d_m, \quad (14)$$

where $J_e = \{m \text{ even integer} | 1 \leq m \leq N_L\}$ and $J_o = \{m \text{ odd integer} | 1 \leq m \leq N_L\}$. Defining the normalized loss angle $\bar{\phi}_c = \phi_c / (\lambda_0 \eta_L)$ and introducing the normalized physical length $z_m = d_m / \lambda_0$, where λ_0 is the free space wavelength, we have:

$$\bar{\phi}_c = \sum_{m \in J_o} \gamma z_m + \sum_{m \in J_e} z_m, \quad (15)$$

where the noise ratio coefficient $\gamma = \eta_H / \eta_L$ can be explicitly written as:

$$\gamma = \frac{\phi_H}{\phi_L} \left(\frac{Y_H}{Y_s} + \frac{Y_s}{Y_H} \right) \left(\frac{Y_L}{Y_s} + \frac{Y_s}{Y_L} \right)^{-1}. \quad (16)$$

In the case where the refractive index n_L is the same as that n_s of the substrate material (as in current GW detectors) N_L is taken as an odd number³.

4.1. Constrained optimization formulation

The optimization of the mirrors for GW detectors is a peculiar problem. In standard mirror optimization design it is important to achieve high reflectance in a given frequency and angular range. In the case of mirrors for GW detectors, the incidence is normal and the frequency range is very narrow (laser signal at $\lambda_0 = 1064 \text{ nm}$) but it is mandatory to find a mirror setup that induces the minimal additional (thermal) noise on the detection channel. Therefore it is important, in a suitable sense, to reduce both the power transmittance $\tau_c = 1 - |\Gamma_c|^2$ and the thermal noise loss angle $\bar{\phi}_c$.

³In fact choosing an even N_L results in a configuration with the right-most layer made of low refractive index material which increases the noise without any effect on the reflectivity.

As a consequence, a straightforward formulation of the coating optimization problem for the design of low noise dielectric mirror can consist in searching for the thickness sequence that minimizes the thermal noise keeping the transmittance below a prescribed threshold value τ_0 . This is a typical constrained optimization problem [23] that in mathematical notation can be written :

$$\begin{aligned} & \text{Minimize}_{z_1, \dots, z_{N_L} \in \Omega} \bar{\phi}_c \\ & \text{subject to} \quad \tau_c \leq \tau_0 \end{aligned} \quad (17)$$

where the constraint transmittance τ_0 should be typically a few part per million (henceforth ppm).

Note that, in view of the transmittance constraint, problem (17) is non-linear and non-convex. The search space Ω is defined by the inequalities $0 \leq z_m \leq 0.25/n_H$ for odd m and $0 \leq z_m \leq 0.5/n_L$ for even m .

An alternative way to formulate the optimization problem can consist in searching for the thickness sequence that minimizes the transmittance keeping the thermal noise below a given threshold value:

$$\begin{aligned} & \text{Minimize}_{z_1, \dots, z_{N_L} \in \Omega} \tau_c \\ & \text{subject to} \quad \bar{\phi}_c \leq \bar{\phi}_0 \end{aligned} \quad (18)$$

where $\bar{\phi}_0$ is a prescribed maximum allowed loss angle.

4.2. Multiobjective optimization formulation

The optimum coating design problem has been formulated in two alternative ways not necessarily equivalent in eq.s (17) and (18). In this section, we introduce a multiobjective optimization approach [24, 25] where we search for the thickness sequences minimizing simultaneously the transmittance and the loss angle. With a non-standard mathematical notation we write:

$$\text{Minimize}_{z_1, \dots, z_{N_L} \in \Omega} [\bar{\phi}_c, \tau_c] \quad (19)$$

Solving problem (19) in the framework of multiobjective optimization means to find its tradeoff curve, also referred as the Pareto front or Pareto boundary, in the $[\bar{\phi}_c, \tau_c]$ plane. Each point belonging to the Pareto front corresponds to a sequence $z_m, m = 1, \dots, N_L$ of layer normalized thicknesses.

In order to define the Pareto front of (19) the concept of *dominance* [24] has to be introduced, to define a suitable

ordering rule in the $[\bar{\phi}_c, \tau_c]$ plane. A physically feasible solution **A** in the space $[\bar{\phi}_c, \tau_c]$ dominates another (different) physically feasible solution **B** if the coordinates of **A** are orderly less or equal to those of **B**. The set of physically feasible solutions, for which no physically feasible dominant solution exists, is the Pareto front of the multiobjective optimization problem. Let us note that the problem (17) can be solved using the Pareto front of (19), by choosing the point on the Pareto front with transmittance component equal to τ_0 . Similar considerations can be done for the problem (18), which can be solved by taking the point on the Pareto front with noise component equal to $\bar{\phi}_0$. Furthermore, the properties and structure of the Pareto front can give some hints on the relationship between problem formulations (17) and (18).

5. Numerical solution of multiobjective optimization problem

Many algorithms, based on different global multiobjective optimization tools, are available in order to face the problem of Pareto front computation for high dimensional problems. These algorithms generally use a suitable sampling method of the physical feasible configuration space, enabling the reconstruction of the Pareto front (e.g. NSGA-II, NSGA-III, ϵ -MOEA etc. see [25]).

In this paper we perform a numerical exploration of the Pareto front (19) using a state of the art, public domain Multi Objective Evolutionary Algorithm (MOEA) named Borg MOEA [17], that uses an evolutionary strategy appropriate for continuous variables. The algorithm is implemented as a package [26] written in the Julia language [27]. The relevant literature and a simple description of the algorithm are reported in Appendix A.

Most multi objective algorithms use mutation, crossover and selection operators, that do not change throughout the execution program. The Borg MOEA uses different operators from existing MOEAs and adopts them adaptively on the basis of their success in the search. The evaluation of the progress, the adaptation of the population size and the increasing of the archive with new solutions help the algorithm to continue the progress and prevents it from being trapped in some loop for the entire runtime. The goodness of numerical solutions given by the Borg MOEA are compared with reference solutions. We consider for comparison with the Borg

Coating	Substrate
H (amorphous Ti-doped Ta ₂ O ₅)	(bulk crystalline SiO ₂)
L (SiO ₂)	
$n_H = 2.10$	$n_s = 1.45$
$n_L = 1.45$	$Y_s = 72 \text{ GPa}$
$\kappa_H = 4.0 \times 10^{-8}$	$\kappa_s = 8.4 \times 10^{-11}$
$\kappa_L = 8.4 \times 10^{-11}$	$\phi_s = 7.00 \times 10^{-8}$
$Y_H = 147 \text{ GPa}$	
$Y_L = 72 \text{ GPa}$	
$\phi_H = 3.76 \times 10^{-4}$	
$\phi_L = 5.00 \times 10^{-5}$	
$\gamma = 9.5$	

Table 1: Physical parameters of coating and substrate materials used in simulations, we assume temperature $T = 300K$ and free space wavelength $\lambda_0 = 1064nm$.

MOEA optimized design, the coating structure which is currently used in Virgo/LIGO test masses [12], consisting of alternating quarter wavelength layers of SiO₂/Ti-doped Ta₂O₅ deposited on a fused silica substrate. The physical parameters used in our simulations are reported in Table 1.

5.1. Pareto front convergence and structure

It is well known that deterministic stopping criteria for global evolutionary optimization algorithms are unavailable. Therefore, in order to investigate the convergence of the used algorithm, we computed the Pareto fronts with $N_L = 11, 15, 19$ for increasing evolution times $T_s = 10^4, 2 \times 10^4, 5 \times 10^4, 10 \times 10^4, 20 \times 10^4$ sec. The numerical estimated maximum absolute deviations (i.e. the uniform norm distance between Pareto curves at T_s and $T_s/2$) are reported in Table 2 showing that the Pareto fronts do not change significantly for $T_s \geq 5 \times 10^4$ sec. As a consequence, we took (*ad abundantiam*) $T_s \sim 10^5$ sec in our simulations.

In Fig. 2(a) we display Pareto fronts for the cases $N_L = 11(2)19$, i.e. ranging from 11 to 19 with step 2. It is seen that the Pareto fronts exhibit several bumps, whose number is equal to the number N_D of high refractive index material layers.

The bumps are less visible in the lower transmittance region. In Fig. 2 (b),(c),(d) the sequences of layer thicknesses corresponding to the square green markers in

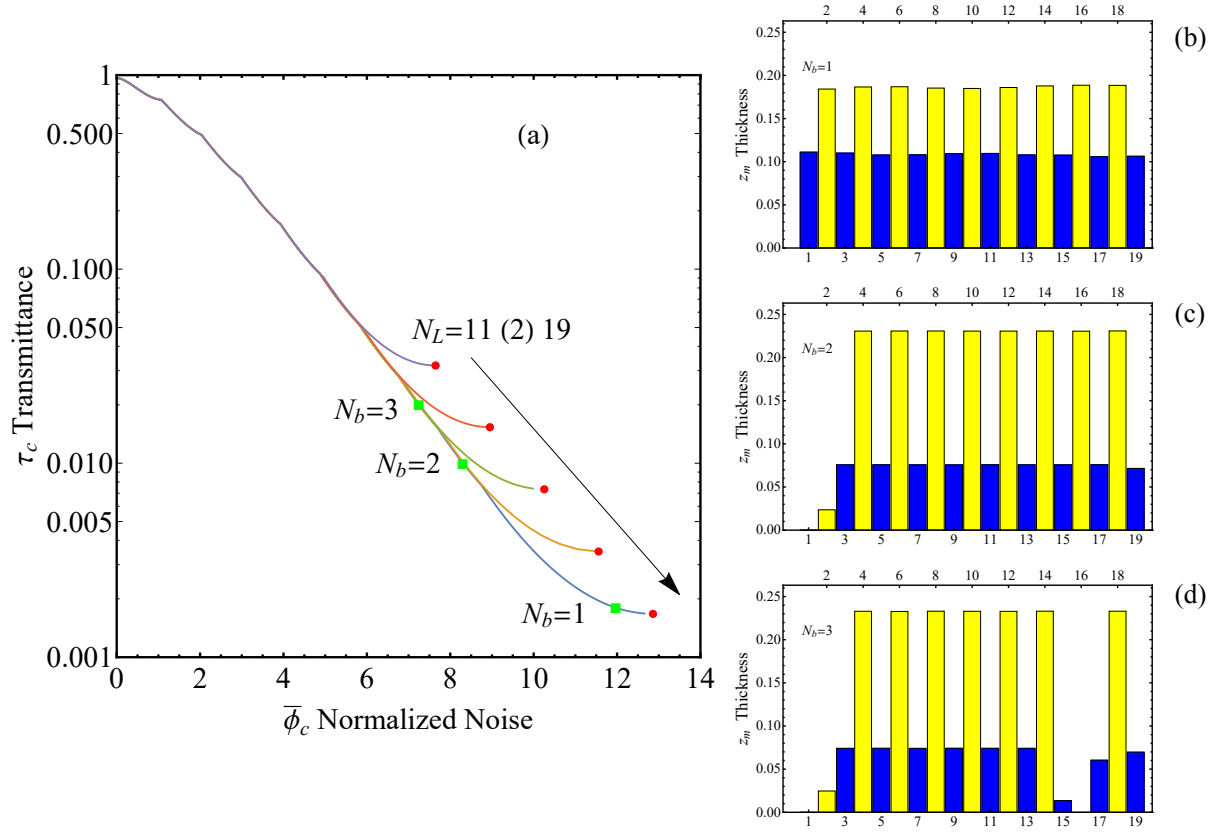


Figure 2: Left panel (a): Pareto fronts for the cases $N_L = 11$ (2) 19. The bump-like structure of Pareto fronts is clearly shown in the high transmittance region of the curve. For the case $N_L = 19$ we indicate with $N_b = 1, 2, 3$ the last three bumps. The red circular markers corresponds to the quarter wavelength design. In the right panel (b,c,d) we display, for the green square markers corresponding to the bumps $N_b = 1, 2, 3$, the thicknesses as a function of layer index m . The height of vertical blue (yellow) bars gives the normalized layer thicknesses z_m of the high (low) refractive index material.

Evolution Time T_s [sec]	Absolute Error
10×10^3	2.3×10^{-3}
20×10^3	1.0×10^{-4}
50×10^3	1.7×10^{-5}

Table 2: Estimated maximum absolute deviation (i.e. numerical estimation of the Pareto fronts distance in the uniform norm) between the Pareto fronts computed at time T_s and the previous one computed at $T_s/2$, for the case $N_L = 19$.

Fig. 2(a) are displayed. It can be noted that the bump with lowest transmittance ($N_b = 1$ in Fig. 2(b)) corresponds to a mirror configuration with all layer thicknesses different from zero. Moreover, we note that the rightmost red point of the bump $N_b = 1$ corresponds to the quarter wavelength design at the operating wavelength $\lambda_0 = 1064 \text{ nm}$ with $N_L = 19$. This is in agreement with the well known quarter wavelength design property of minimizing transmittance in the cases of multilayer reflectors made of negligibly absorbing materials [28]. The next bump $N_b = 2$ corresponds to a mirror design where the thickness of a single layer of high refractive index has been *practically* set to zero (see Fig. 2(c)). For the case $N_b = 3$ illustrated in Fig. 2(d), the thickness of an additional layer of low index material is set to zero; this implies that the two nearby high refractive index layers merge together and can be considered as a single layer. We found that the above behaviour can be generalized to all bumps, i.e. the generic bump $N_b = k$ fairly corresponds to a multilayer structure with $N_D - k + 1$ high refractive index layers.

This feature is a general characteristic of the Pareto front of dielectric mirror multiobjective optimization, which are, in summary, continuous, decreasing, and non-convex (*bumpy*) curves. The continuity of multiobjective tradeoff curves implies that the problems (17) and (18) are mathematically equivalent. In fact if we consider a generic point $[\bar{\phi}_0, \tau_0]$ on the Pareto front, we find that $\bar{\phi}_0$ is the solution of problem (17) with constraint τ_0 , while τ_0 is the solution of problem (18) with constraint $\bar{\phi}_0$.

In order to consider design configurations that exhibit performances of potential interest for present GW interferometer detectors, we performed simulations for coating multilayer up to $N_L = 39$ with the physical parameters reported in Table 1. In Fig. 3 we display the Pareto curves (blue lines) for N_L ranging from 11 to 39 with step

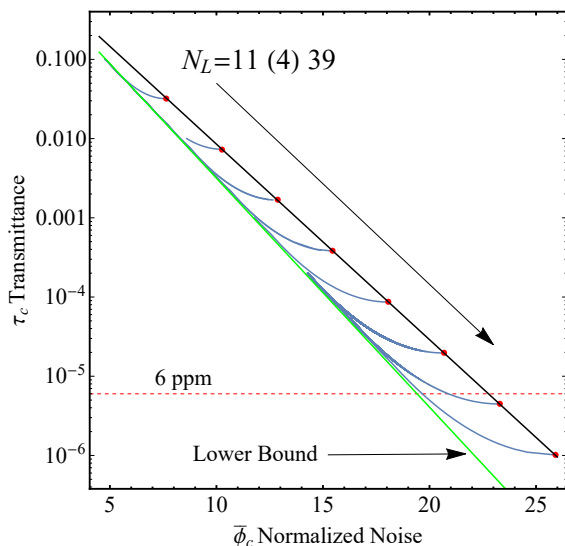


Figure 3: Pareto fronts for $N_L = 11$ to $N_L = 39$ in step of 4 in log-linear scale (blue curves). The simulation parameters are reported in Table 1. Red circular markers refer to the quarter wavelength design. The dashed red horizontal grid line at $\tau_c = 6 \text{ ppm}$ is the typical design target of 2nd generation (advanced) Virgo-LIGO detectors. The black line corresponds to equation (20) computed with simulation parameters of Table 1, the green line labeled "Lower Bound" is the same eq. (20) with an *effective* noise ratio coefficient $\gamma_e = 7.9$.

4. The red points in Fig. 3 are the quarter wavelength design which are located on a curve that can be written (under some approximations) as a straight line in the log-linear axes scale of the plane $[\bar{\phi}_c, \tau_c]$. The equation of the straight line is (see Appendix B for details):

$$\log(\tau_c) = \log\left(\frac{4}{n_L}\right) - \frac{2n_H}{\gamma n_L + n_H} \log\left(\frac{n_H}{n_L}\right) + \bar{\phi}_c \frac{8n_L n_H}{\gamma n_L + n_H} \log\left(\frac{n_H}{n_L}\right). \quad (20)$$

The tradeoff curves asymptotically locate near to a straight line (green line in Fig. 3) in the plane $[\bar{\phi}_c, \tau_c]$ with a log-linear axes scale. The equation of this line turns out to be the same eq. (20) where the noise ratio coefficient is reduced to an *effective* value $\gamma_e = 7.9$, computed by regression of Pareto front data. We conjecture that this curve is a lower bound for all tradeoff curves in the region of low transmittance ($\tau_c \leq 0.1$) above the Koppelman limit [29], that is placed at $\tau_c \sim 10^{-7}$ for the parameters reported in Table 1. The Koppelman limit is also the order of magnitude of normalized energy absorption (*absorbance*) in the sought design in Fig. 2(b)(c)(d) and in the following.

The horizontal dashed red line $\tau_c = 6$ ppm shown in Fig. 3 corresponds to the target transmittance required for the design of dielectric mirrors used in GW detectors. The quarter wavelength coating with $N_L = 35$ is the reference design because it matches the target transmittance with the lowest normalized noise.

It is clear that each tradeoff curve with $N_L \geq 35$ contains layer configurations satisfying the constraint $\tau_c \leq 6$ ppm and showing a reduced normalized noise $\bar{\phi}_c$ with respect to the quarter wavelength reference design.

In figure 4(a)(b)(c) the layer thickness configurations obtained by the intersections between tradeoff curves with $N_L = 39, 41, 43$ and the horizontal transmittance line $\tau_c = 6$ ppm are displayed. These configurations give a reduction of the normalized noise with the respect to the quarter wavelength reference design of about 15.5%, 15.9%, 15.9% respectively. Note that the designs reported in Fig. 4(a) and 4(b) belong to the first bump of the tradeoff curves $N_L = 39, 41$ respectively, while the configuration in Fig. 4(c) belongs to the second bump of the Pareto front $N_L = 43$.

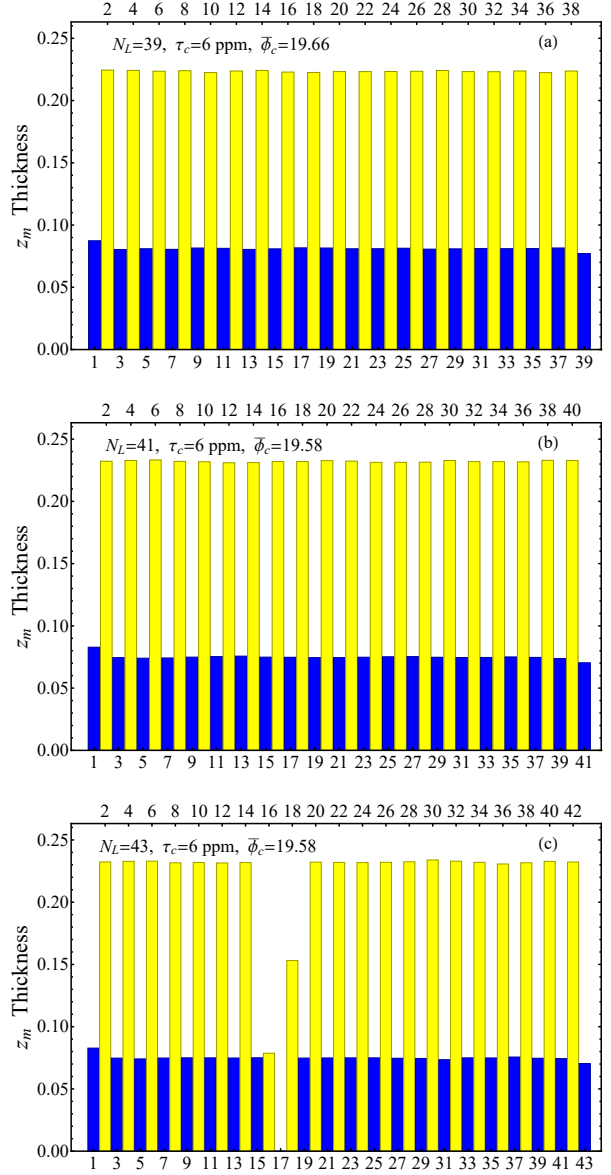


Figure 4: From top (a) to bottom (c) the normalized layer thicknesses z_m of the optimal multiobjective design for cases $N_L = 39, 41, 43$. The height of vertical blue bars gives the normalized layer thicknesses z_m of high refractive index material (odd m values on the bottom axis). The height of vertical yellow bars gives the normalized layer thicknesses z_m of the low refractive index material (even m values on the top axis). The design corresponds to the points obtained by the intersection of the Pareto boundary with the horizontal line (dashed line in Fig. 3) drawn at the prescribed transmittance level ($\tau_c = 6$ ppm).

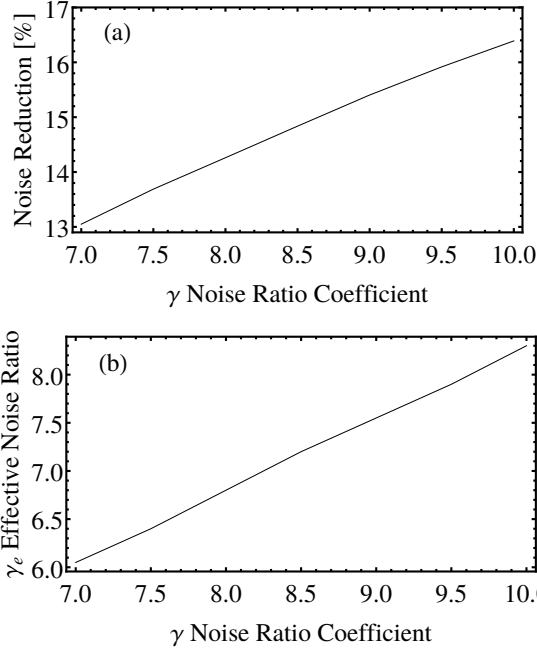


Figure 5: (a) The percent loss angle reduction of the optimized coatings with respect to the reference quarter wavelength design. (b) The effective noise ratio coefficient γ_e as a function of γ , computed by fitting eq. (20) to the Pareto front.

Moreover, let us note that the thickness sequences look like a truncated periodic configuration except for the first two layers and the last one. The normalized physical length of the internal layers with high and low refractive index materials are $z_H \sim 0.081$ and $z_L \sim 0.22$, respectively, corresponding to normalized optical lengths $n_H z_H \sim 0.17$ and $n_L z_L \sim 0.32$, whose sum is less than 0.5.

In view of the uncertainty in the measurements of the specific loss angle coefficient, we have performed all the above simulations considering the same refractive indexes n_H , n_L and n_s (see Table 1) and changing the noise ratio coefficient in the range $\gamma \in [7, 10]$. All of the above findings are confirmed. We report in Fig. 5 a summary of the relevant results. In particular, the noise reduction of the optimized coating structure with respect to the reference quarter wavelength design and the effective γ_e noise ratio coefficient are reported as functions of γ in Fig. 5(a) and

Parameters	$\bar{\phi}_c$ Periodic	$\bar{\phi}_c$ Tweaked	$\bar{\phi}_c$ Borg MOEA
$N_L = 19$ $\tau_c = 6 \times 10^{-3}$	9.1214	9.1054	9.1054
$N_L = 27$ $\tau_c = 10^{-4}$	16.5918	16.5879	16.5879
$N_L = 41$ $\tau_c = 6 \times 10^{-6}$	19.5968	19.5809	19.5809

Table 3: Normalized noise $\bar{\phi}_c$ of the optimum design. The target transmittance τ_c and the number of layers N_L are reported in the first column. For these parameters, the minimal loss angles, obtained with different optimization procedures are displayed in the other columns.

5(b), respectively. We have shown that both the noise reduction (*gain*) and the effective noise ratio γ_e are almost linear, increasing functions of the noise ratio coefficient γ .

The above parametric exploration has been done exploiting the possibility in reducing the computational burden for the calculation of the limiting curve of Pareto fronts. Indeed the bound given by eq. (20) can be evaluated only for two value of N_L in a moderately low τ_c region, and then extrapolated via mono-parametric regression to the whole low transmittance region above the Koppelman limit.

5.2. The tweaked periodic solution and the mixture checks

We have found that the thickness sequences look like a truncated periodic configuration with the exception of the two topmost layers and the last one. This result corroborates the working hypothesis used in previous papers [14, 15]. As a further check, we have implemented a code to face the tweaked periodic truncated design problem where the search space Ω is reduced to a five-dimensional space by setting $z_1 = x_1$, $z_2 = x_2$, and $z_{N_L} = x_5$ for the first two layers and the last one in the dielectric mirror. In the remaining layers for all m odd in the range $N_L > m > 1$ we set $z_m = x_3$, and for all m even in the range $N_L > m > 2$ we set $z_m = x_4$. In Table 3 we report the tweaked and the complete multiobjective solutions. We note that in terms of noise reduction an agreement on the first four decimal figures is found. We have also considered the periodic truncated design with a two-dimensional search space Ω .

The results shown in Table 3 evidentiate a deviation of the periodic truncated design with respect to the full evolutionary solution. This difference in the tradeoff curve increases in the low transmittance region.

A final check has been carried out in order to verify whether it is convenient to substitute the high refractive index material (noisier material) with a layered mixture of this material and the low index one. To this end we expand the search space including for the high refractive layers (modeled like a mixture with layered inclusion) an additional variable ξ_i which account for the percent of high refractive index material present in the layered mixture. In the case of layered inclusion the mixture refractive index can be modeled following [30, 31] and is $\sqrt{n_H^2 \xi_i + n_L^2 (1 - \xi_i)}$, while the normalized thermal noise ratio becomes $\gamma \xi_i + (1 - \xi_i)$. The multiobjective simulations performed in the expanded $N_L + N_D$ -dimensional space Ω , using the same parameters of Table 1 and for different values of N_D , shown that the Pareto tradeoff curve does not change because the algorithm automatically finds that $\forall i : \xi_i \sim 1$. This result implies that mirror design made of *true* (i.e. with $\xi_i < 1$) layered mixture solutions are located above the binary coating Pareto fronts.

The failure of this check definitively gives an answer on the optimality of mirror design with subwavelength layered inclusions in the case of coatings made of two materials, and also establish that it is not convenient to arbitrarily increase N_L , keeping fixed τ_c , to search the optimal solutions.

6. Conclusions

In this article we faced the problem of optimizing the design of binary (two-materials) coatings for GW detectors by formulating and solving a multiobjective optimization problem. This approach allowed us to minimize both the transmittance and the thermal noise. While the values of the refractive indexes and the number of the layers are given, no *a priori* hypothesis on the thickness of the layers was made in the multiobjective optimization problem, tackled using a global optimization method (Borg MOEA) in a search space with a dimension equal to the number of layers.

We have shown by extensive numerical simulation based on Borg MOEA algorithm the existence of a Pareto

tradeoff boundary which is a continuous, decreasing, and non-convex (bump-like) curve. In particular, continuity implies that the multiobjective approach (19) is equivalent to the constrained single-objective optimization problems (17) and (18). A solution (i.e. a mirror design) on the Pareto front corresponds to a sequence of layer thicknesses.

The thicknesses sequences on the Pareto boundary look like truncated periodic configurations except for the first two layers and the last one. In view of this result (see also [14]), we faced the optimization problem in a search space with a reduced dimension. We have considered the adapted periodic (five-dimensional search space) and the truncated periodic (two-dimensional search space) sequence. The performance of the tweaked (adapted) periodic sequences are comparable to the performance of the sequences obtained by the solution of the full multiobjective problem. The periodic design is outperformed by the multiobjective design especially in the low transmissivity region.

We have also shown that the Pareto fronts are bounded from below by an exponential curve in the transmittance-noise plane (20). This curve has the same expression of the approximate relation between transmittance and noise for the quarter wavelength design, except for the noise ratio coefficient which assumes a reduced *effective* value. A possible application of eq. (20), consisting in the reduction of the computational burden for the calculation of the Pareto fronts, has been implemented for a parametric exploration in a suitable γ range.

The noise reduction ($\sim 16\%$ for realistic cases) has been shown to be (more or less) a linear, increasing function of the noise ratio coefficient γ .

There is no possibility to ameliorate these performances by using instead of high refractive index material a mixture made of layered inclusions of low refractive index material, with subwavelength thicknesses, placed inside the high refractive index material.

We are confident that the method used in this paper can be generalized to the analysis of the coating design of dielectric mirror with three or more different materials, to be discussed in a future paper.

Acknowledgments

This work has been partially supported by INFN through the projects Virgo and Virgo–ET. M. Principe acknowledges the L’Oreal-UNESCO For Women in Science Program for supporting her in this work. The authors are grateful for the discussion and suggestions received from the Virgo Coating R&D Group and the Optics Working Group of the LIGO Scientific Collaboration.

Appendix A - evolutionary algorithm in a nutshell

The evolutionary algorithms are smart versions of random search derived from the genetic evolution theory and implemented on digital computers. They are well established classical tools for global optimization techniques [32].

To solve optimization problems with an evolutionary algorithm the individuals of a population are associated, by the encoding procedure, to a physical solution of a given problem (in our case the layer thicknesses sequence), the selection probability is proportional to the quality of the represented solution, i.e. to the fitness function to be optimized.

The population then undergoes selection crossover and mutation (like in natural genetics evolution), producing new children and updating the population. The process is repeated over various generations until a suitable termination criteria is reached. Each individual, encoding a candidate solution, is assigned a fitness value, based on its objective function value, and the fitter individuals are given a higher chance to mate and yield more *fitter* individuals.

The multi objective version of evolutionary algorithm follows the same schema (see [24, 25] for details), with the addition of a suitable strategy of Pareto front extraction.

An evolutionary heuristic follows this basic scheme:

Algorithm 1: Multi-Objective evolutionary algorithm

Result: Pareto front of population
initialize random population $P(0)$, at the iteration
 $t = 0$;
find fitness of initial population;
extraction of Pareto front elements;
while *termination criteria is not reached* **do**
 parent selection;
 crossover of the parent;
 mutation;
 decode and fitness calculation;
 survivor selection and update population $P(t + 1)$;
 extraction of Pareto front elements from $P(t + 1)$;
 increment t ;
return Pareto fronts;

We address the reader to the cited literature [17, 26] for a detailed description of the used algorithm.

Appendix B - transmittance vs thermal noise for the quarter wavelength design

In this appendix we compute the transmittance as a function of thermal noise for a quarter wavelength coating. The reflectivity of a quarter wavelength multilayer made of $N_L = 2N_D - 1$ alternating layers with high and low refractive indexes n_H and n_L , respectively, placed on a substrate with refractive index $n_s = n_L$ is:

$$|\Gamma_c|^2 = \frac{\left(1 - n_L \left(\frac{n_H}{n_L}\right)^{2N_D}\right)^2}{\left(1 + n_L \left(\frac{n_H}{n_L}\right)^{2N_D}\right)^2} \quad (21)$$

where $n_H/n_L \geq 1$. In view of eq. (21) the transmittance $\tau_c = 1 - |\Gamma_c|^2$ reads:

$$\tau_c = \frac{4n_L \left(\frac{n_H}{n_L}\right)^{2N_D}}{\left(1 + n_L \left(\frac{n_H}{n_L}\right)^{2N_D}\right)^2} \quad (22)$$

that can be written as

$$\tau_c = \frac{\frac{4}{n_L} \left(\frac{n_H}{n_L}\right)^{-2N_D}}{\left(1 + \frac{1}{n_L} \left(\frac{n_L}{n_H}\right)^{2N_D}\right)^2} . \quad (23)$$

For $\frac{1}{n_L} \left(\frac{n_L}{n_H}\right)^{2N_D} \ll 1$, by applying the log on both side of the equation (23) we get

$$\log(\tau_c) \sim \log\left(\frac{4}{n_L}\right) - 2N_D \log\left(\frac{n_H}{n_L}\right). \quad (24)$$

On the other hand, specializing eq. (15) for the quarter wavelength design, the normalized loss angle $\bar{\phi}_c$ can be written as a function of N_D

$$\bar{\phi}_c = \frac{\gamma N_D}{4n_H} + \frac{N_D - 1}{4n_L} = \left(\frac{\gamma}{4n_H} + \frac{1}{4n_L}\right)N_D - \frac{1}{4n_L}. \quad (25)$$

Solving (25) for N_D and plugging into (24) we have:

$$\log(\tau_c) \sim \log\left(\frac{4}{n_L}\right) - \frac{2n_H}{\gamma n_L + n_H} \log\left(\frac{n_H}{n_L}\right) + \bar{\phi}_c \frac{8n_L n_H}{\gamma n_L + n_H} \log\left(\frac{n_H}{n_L}\right). \quad (26)$$

References

References

- [1] website <http://www.ligo.caltech.edu>
- [2] website <http://www.virgo.infn.it>
- [3] B.P. Abbott, et al., *Multi-messenger Observations of a Binary Neutron Star Merger*, Ap. J. Lett. 848 (2017) L12.
- [4] M. Branchesi, *Multi-messenger astronomy: gravitational waves, neutrinos, photons, and cosmic rays*, J. Phys. Conf. Ser. 718 (2016) 022004.
- [5] M. R. Abernathy, X. Liu, T. H. Metcalf, An overview of research into low internal friction optical coatings by the gravitational wave detection community, Materials Research 21 (2018) e20170864.
- [6] R. Flaminio, J. Franc, C. Michel, N. Morgado, L. Pinard, B. Sassolas, *A study of coating mechanical and optical losses in view of reducing mirror thermal noise in gravitational wave detectors*, Class. Quantum Grav. 27 (2010) 084030.

- [7] G.D. Cole, W. Zhang, B. J. Bjork, D. Follman, P. Heu, C. Deutsch, L. Sonderhouse, J. Robinson, C. Franz, A. Alexandrovski, M. Notcutt, O. H. Heckl, J. Ye, M. Aspelmeyer, *High-performance near- and mid-infrared crystalline coatings*, Optica 3 (2016) 647-656.
- [8] H.-W. Pan, S.-J. Wang, L.-. Kuo, S. Chao, M. Principe, I. M. Pinto, R. DeSalvo, Thickness-dependent crystallization on thermal anneal for titania/silica nm-layer composites deposited by ion beam sputter method, Optics Expr. 22 (2014) 29847-29854.
- [9] H.-W. Pan, L.-C. Kuo, S.-Y. Huang, M.-Y. Wu, Y.-H. Juang, C.-W. Lee, H.-C. Chen, T. T. Wen, S. Chao, *Silicon nitride films fabricated by a plasma-enhanced chemical vapor deposition method for coatings of the laser interferometer gravitational wave detector*, Phs. Rev. D 97 (2018) 022004.
- [10] J. Steinlechner, C. Krüger, I. W. Martin, A. Bell, J. Hough, H. Kaufer, S. Rowan, R. Schnabel, S. Steinlechner, *Optical absorption of silicon nitride membranes at 1064 nm and at 1550 nm*, Phys. Rev. D 96 (2017) 022007.
- [11] L. Pinard, B. Sassolas, R. Flaminio, D. Forest, A. Lacoudre, C. Michel, J. L. Montorio, N. Morgado, *Toward a new generation of low-loss mirrors for the advanced gravitational waves interferometers*, Optics Letters 36 (2011) 1407-1409.
- [12] L. Pinard, C. Michel, B. Sassolas, L. Balzarini, J. Degallaix, V. Dolique, R. Flaminio, D. Forest, M. Granata, B. Lagrange, N. Straniero, J. Teillon, G. Cagnoli, *Mirrors used in the LIGO interferometers for first detection of gravitational waves*, Applied Optics 56 (2017) C11-C15.
- [13] G. Harry, T. P. Bodiya, R. DeSalvo, *Optical coatings and thermal noise in precision measurements*, Cambridge University Press, 2012.
- [14] J. Agresti, G. Castaldi, R. DeSalvo, V. Galdi, V. Pierro, I. M. Pinto, *Optimized multilayer dielectric mirror coatings for gravitational wave interferometers*, Proc. of SPIE 6286 (2006) 628608.

- [15] A.E. Villar, E. D. Black, R. DeSalvo, K. G. Libbrecht, C. Michel, N. Morgado, L. Pinard, I. M. Pinto, V. Pierro, V. Galdi, M. Principe, I. Taurasi, *Measurement of thermal noise in multilayer coatings with optimized layer thickness*, Phys. Rev. D 81 (2010) 122001.
- [16] N. M. Kondratiev, A. G. Gurkovsky, M. L. Gorodetsky, *Thermal noise and coating optimization in multilayer dielectric mirrors*, Phys. Rev. D 84 (2011) 022001.
- [17] D. Hadka , P.M. Reed , *Borg: An Auto-Adaptive Many-Objective Evolutionary Computing Framework*, Evolutionary Computation 21 (2013) 231-259.
- [18] F. Abelès, *La théorie générale des couches minces*, Le Journal de Physique et le Radium, 11 (1950) 307-310.
- [19] M. Born , E. Wolf , *Principles of Optics: Electromagnetic Theory of Propagation, Interference and Diffraction of Light.*, Cambridge University Press 1997.
- [20] S. J. Orfanidis , *Electromagnetic Waves and Antennas*, available as web book <https://www.ece.rutgers.edu/~orfanidi/ewa/>.
- [21] A. Allocca, A. Gatto, M. Tacca, R. A. Day, M. Barsuglia, G. Pillant, C. Buy, C., G. Vajente, *Higher-order Laguerre-Gauss interferometry for gravitational-wave detectors with in situ mirror defects compensation*, Phys. Rev. D 92 (2015) 102002.
- [22] I.W. Martin E. Chalkley, R. Nawrodt, H. Armandula, R. Bassiri, C. Comtet, M. M. Fejer, A. Gretarsson, G. Harry, D. Heinert, J. Hough, I. MacLaren, C. Michel, J-L Montorio, N. Morgado, S. Penn, S. Reid, R. Route , S. Rowan, C. Schwarz , P. Seidel , W. Vodel, A. L. Woodcraft, *Comparison of the temperature dependence of the mechanical dissipation in thin films of Ta2O5 and Ta2O5 doped with TiO2*, Class. Quantum Grav. 26 (2009) 155012.
- [23] A. Antoniou, W. S. Lu, *Practical Optimization - Algorithms and Engineering Applications*, Springer, Boston, MA, USA 2007.
- [24] M.T.M. Emmerich , A.H. Deutz, *A tutorial on multi-objective optimization: fundamentals and evolutionary methods*, Natural Computing 17 (2018) 585-609 .
- [25] D. Kalyanmoy, *Multi-Objective Optimization Using Evolutionary Algorithms*, John Wiley and Sons, Inc. New York, NY, USA 2001.
- [26] R. Feldt, BlackBoxOptim, GitHub repository <https://github.com/robertfeldt/BlackBoxOptim.jl> (2019).
- [27] website <https://julialang.org>
- [28] C. K. Carniglia , J. H. Apfel , *Maximum reflectance of multilayer dielectric mirrors in the presence of slight absorption*, J. Opt. Soc. Am. 70 (1980) 523-534.
- [29] G. Koppelman, *On the theory of multilayers consisting of weakly absorbing materials and their use as interferometric mirrors*, Ann. Phys. 5 (1960) 388-396.
- [30] A. Sihvola, *Electromagnetic Mixing Formulas and Applications*, The Institution of Engineering and Technology, London, United Kingdom 2008.
- [31] M. Kar , B. S. Verma, A. Basu , R. Bhattacharyya, *Modeling of the refractive index and extinction coefficient of binary composite films*, Applied Optics 40 (2001) 6301-6306.
- [32] J. H. Holland, *Adaptation in Natural and Artificial Systems*, University of Michigan Press, 1975.